Resonance Raman Overtone Intensities and Electron-Phonon Coupling Strengths in Semiconductor Nanocrystals

Anne Myers Kelley*

Chemistry & Chemical Biology, University of California, Merced, 5200 North Lake Road,

Merced, CA 95343

Tel: (209) 228-4345

E-mail: amkelley@ucmerced.edu

Abstract

For linear electron-phonon coupling, the Huang-Rhys factor, S, gives the intensity ratio of the one-quantum vibronic transition (0→1) to the purely electronic origin transition (0→0) in a vibrationally resolved, zero-temperature absorption or emission spectrum. It is often assumed that the overtone to fundamental integrated intensity ratio in resonance Raman scattering of semiconductor nanocrystals is equal to or proportional to S, or that S may be determined from the overtone intensity in some other straightforward manner. In fact, this is not generally possible because of different excitation profiles for overtones and fundamentals, differential sensitivity of overtones and fundamentals to electronic dephasing, and interference effects from partially overlapping electronic transitions. Here we examine the relationship between the Huang-Rhys factor and the overtone to fundamental intensity ratio through spectroscopic simulations using parameters appropriate to II-VI semiconductor nanocrystals such as CdSe. A simple equation relating the overtone to fundamental Raman intensity ratio to the Huang-Rhys factor is obtained only in the case of a single resonant electronic state, excitation at the maximum of the inhomogeneously broadened absorption band, and a homogeneous linewidth small compared with the phonon frequency.

Keywords: cadmium selenide; Huang-Rhys factor; resonance Raman excitation profile; homogeneous broadening; dephasing

1. INTRODUCTION

Electron-phonon coupling (EPC) may be defined as the extent to which distortion of the nuclei along a vibrational coordinate changes the energy separation between two electronic states. In the simplest case, the potential energy surfaces for different electronic states differ only by a constant plus a term linear in one or more nuclear coordinates (normal modes). This is referred to as linear electron-phonon coupling. The strength of the EPC is expressed by the Huang-Rhys factor, S, given by $\Delta^2/2$ where Δ is the difference between the potential minima of the two electronic states along the ground-state dimensionless normal coordinate.[1-4] (With this definition, $\Delta = 1$ when the two potential energy surfaces are displaced by $\sigma/\sqrt{2}$ where σ is the standard deviation of the probability distribution in the ground vibrational state, $|\Psi_0|^2$. Some workers[5-8] use an alternative definition in which Δ is smaller by $\sqrt{2}$, and $S = \Delta^2$.) The magnitude of EPC influences a number of optical, photophysical, and transport properties that are of interest in semiconductor nanocrystals (SC NCs) including the Stokes shift between absorption and emission, the efficiency of multiple exciton generation, and the rates of electron and hole transfer through the material and across interfaces.[9-14]

In a vibrationally resolved, zero-temperature absorption or emission spectrum where the optical transition originates entirely from the vibrationless state, the Huang-Rhys factor determines the intensities of the vibronic sub-bands making up the electronic transition. Specifically,

$$\frac{I_{0\to v}}{I_{0\to 0}} = \frac{|\langle v|0\rangle|^2}{|\langle 0|0\rangle|^2} = \frac{S^v}{v!} \qquad (1)$$

For $S < 1$, most of the intensity of the electronic transition is in the origin band, with a weaker $0 \to 1$ transition and progressively weaker $0 \to v$ bands; for $S > 1$, the vibronic intensity first

increases with increasing v, reaching a maximum at v = S, and then decreases for larger v. The ratio of the one-quantum vibronic transition to the electronic origin is given by S, and the ratio of the two-quantum (overtone) to one-quantum (fundamental) transition is given by S/2. Therefore it should be possible to determine the EPC strength simply by inspecting a resolved electronic spectrum; however, absorption or emission spectra of SC NCs exhibiting adequate resolution are seldom available because of the inhomogeneous broadening present in even the most monodisperse NC preparations. While there are examples of the determination of S from photoluminescence and/or excitation spectra of single NCs[15,16] as well as ensembles,[17-19] such measurements remain challenging.

An experimentally easier way to measure vibronic intensities is through resonance Raman scattering. The matrix element for a $0 \rightarrow v$ phonon transition in a resonance Raman spectrum depends on the EPC strength for each phonon. It is often assumed that the ratio of the integrated area of the first overtone transition to that of the fundamental, $I_{0\rightarrow2}/I_{0\rightarrow1}$, is equal to or directly proportional to S,[20-26] as it is in one-photon absorption or emission as described above. However, this is not generally the case for resonance Raman scattering, a coherent two-photon process in which paths through different intermediate states interfere. In its simplest "sum-over-states" formulation, the resonance Raman cross-section for a molecule or NC initially in its vibrationless ground state can be written as[3]

$$\sigma(\omega_L) \propto \omega_L \omega_S^3 |M|^4 \left| \sum_V \frac{\langle F|V\rangle\langle V|0\rangle}{\omega_0+\omega_V-\omega_L-i\Gamma} \right|^2 \qquad (2)$$

where M is the electronic transition dipole moment between the ground state and the resonant excited state having purely electronic transition frequency ω_0, F is the final state in the Raman process, V is a phonon level of the resonant excited state having vibrational frequency ω_V, ω_L

and ω_S are the incident and scattered frequencies, and Γ is the homogeneous linewidth (lifetime plus dephasing width) characterizing the electronic transition. In the linear electron-phonon coupling limit, the vibrational overlap integrals in the numerator have the following simple forms for Rayleigh, Raman fundamental, and Raman overtone scattering, respectively:[27]

$$\langle 0|V\rangle\langle V|0\rangle = \frac{e^{-S}S^{v}}{v!} \tag{3a}$$

$$\langle 1|V\rangle\langle V|0\rangle = \frac{1}{\sqrt{2}}\left\{\Delta - \frac{2V}{\Delta}\right\}\langle 0|V\rangle\langle V|0\rangle \tag{3b}$$

$$\langle 2|V\rangle\langle V|0\rangle = \frac{1}{\sqrt{2}}\left\{S - 2V + \frac{V(V-1)}{S}\right\}\langle 0|V\rangle\langle V|0\rangle \tag{3c}$$

Eq. (2) involves first summing the complex-valued contributions from each intermediate state V and then taking the modulus squared. Contributions from different intermediate states can interfere either constructively or destructively in a manner that depends not only on the EPC strength but also on the excitation wavelength and the linewidth. Thus, estimating S from an experimental overtone to fundamental Raman intensity ratio requires, at minimum, assumptions about the electronic resonance frequency and the homogeneous linewidth, and consideration of the distribution of resonance frequencies that arises from inhomogeneities in NC size and/or shape. These issues were addressed in early resonance Raman studies on SC NCs,[1,5-7,28] but appear to have been largely ignored or misunderstood in much recent work.

Most resonance Raman experiments on SC NCs are also subject to additional complexities not considered in previous studies. First, rarely does a single excitonic transition contribute to the resonance enhancement at any given excitation wavelength. In most SC NCs there is strong experimental and/or theoretical evidence for multiple overlapping transitions, although little may be known about the relative EPC strengths for these different transitions. The oscillator

strength and polarization direction of each transition must be taken into account in order to properly capture the interference effects among different transitions. Second, many SC NCs have Raman frequencies that are not low compared with k_BT at the temperature of the experiment, so the effect of hot bands on the Raman intensities must be considered. Third, many of the mechanisms that contribute to rapid homogeneous dephasing in condensed phases near room temperature are not adequately described by simple exponential decay of the photoinduced coherence, which would give a very broad Lorentzian lineshape for the electronic transition. Physically more reasonable models such as the Brownian oscillator[4,29,30] generate a dephasing decay that may be exponential at long times but is more nearly Gaussian or inertial at short times, and the effect of dephasing on resonance Raman scattering is not as simple as the $i\Gamma$ appearing in the denominator of eq. (2).

In this paper we present a set of model calculations that explore the effects of homogeneous and inhomogeneous electronic spectral broadening, overlapping electronic transitions, and nonzero temperature on the overtone to fundamental intensity ratio in resonance Raman scattering. The parameters used in these calculations are roughly appropriate for CdSe quantum dots, one of the earliest SC NC systems for which resonance Raman profiles were reported;[5] however, we expect that the qualitative results should be applicable to other NC materials and morphologies as well.

2. COMPUTATIONAL METHODS

Eq. (2) for the resonance Raman cross-section assumes a single resonant electronic transition, zero temperature, and purely Lorentzian homogeneous broadening of the resonant

electronic transition. While multiple resonant transitions, inhomogeneous broadening of the electronic transitions, and thermal population of initial vibrational states may be accounted for straightforwardly within the sum-over-states framework of eq. (2),[3] the homogeneous broadening resulting from physically reasonable models for electronic dephasing is very messy to incorporate within a sum-over-states formalism.[31,32] Therefore, we employ the "time-domain" formulation of resonance Raman scattering[3,4,33] to calculate Raman excitation profiles and optical absorption spectra. This is mathematically equivalent to the sum-over-states approach, but it is computationally more tractable when non-exponential homogeneous dephasing and/or large numbers of coupled vibrational modes need to be considered.[3,34]

The computational methods have been described in detail in previous publications.[4,35,36] For application to CdSe nanocrystals in the wurtzite crystal structure, where there is one unique axis,[37] each of the electronic states contributing to the optical absorption or Raman enhancement was assumed to be polarized either along the z axis or degenerate in the xy plane. The Condon approximation was assumed, whereby the transition dipole moment to an excited vibronic state separates into the product of a purely electronic transition dipole and a purely vibrational overlap integral. For direct-gap semiconductors such as CdSe, where the optical transition is fully electronically allowed and very strong (oscillator strengths typically exceeding unity), the Condon approximation is expected to hold for the same reasons that it does for molecules with strongly allowed transitions. We assume the common experimental configuration in which the incident excitation is linearly polarized (*e.g.* along $\hat{z}$) and propagates along $\hat{x}$, and the scattered light is detected propagating along $\hat{y}$ and polarized either parallel ($\hat{z}$) or perpendicular ($\hat{x}$) to the incident polarization. The differential Raman cross sections for parallel and perpendicular

polarization detection for a transition between vibrational levels I and F is given by[36,38] (in SI units)[39]

$$\left[\frac{d\sigma_{IF}(\omega_L,\delta)}{d\Omega}\right]_{||} =$$

$$\frac{\omega_L\omega_S^3}{16\pi^2\varepsilon_0^2\hbar^2c^4}\frac{1}{15}\left[8\left|\alpha_{xx,IF}(\omega_L,\delta)\right|^2+3\left|\alpha_{zz,IF}(\omega_L,\delta)\right|^2+4Re\left[\alpha^*_{xx,IF}(\omega_L,\delta)\alpha_{zz,IF}(\omega_L,\delta)\right]\right] \quad (4a)$$

$$\left[\frac{d\sigma_{IF}(\omega_L,\delta)}{d\Omega}\right]_{\perp} =$$

$$\frac{\omega_L\omega_S^3}{16\pi^2\varepsilon_0^2\hbar^2c^4}\frac{1}{15}\left[\left|\alpha_{xx,IF}(\omega_L,\delta)\right|^2+\left|\alpha_{zz,IF}(\omega_L,\delta)\right|^2-2Re\left[\alpha^*_{xx,IF}(\omega_L,\delta)\alpha_{zz,IF}(\omega_L,\delta)\right]\right] \quad (4b)$$

where ω_L and ω_S are the laser and scattered frequencies. The components of the Raman polarizability tensor are calculated in the time domain as[4]

$$\alpha_{kk,IF}(\omega_L,\delta)=\sum_e M_{e,k}^2\int_0^\infty dt\,\langle F|I(t)\rangle_e\,exp\left[i\left(\omega_L-\omega_{eg}-\delta+\omega_I\right)t-g_e(t)\right] \quad (5)$$

where e is an electronic (electron-hole) state, $M_{e,k}$ is the electronic transition dipole moment between the ground state and excited state e along direction k (in a nanocrystal-fixed coordinate system), ω_{eg} is the central frequency difference between the purely electronic states, δ is a shift in this frequency for different members of an inhomogeneous ensemble (see below), and $g_e(t)$ is a damping function that accounts for all sources of electronic homogeneous dephasing. As discussed further below, we model the homogeneous dephasing as coupling to an overdamped Brownian oscillator,[30,40] with the explicit expression for $g_e(t)$ given in eqs. (8.48) of ref. 40. The quantity $|I(t)\rangle_e = e^{-iH_et/\hbar}|I\rangle$ is the initial ground-state phonon wavefunction propagated on the potential energy surface for excited state e.

In order to account for the distribution in transition frequencies caused by a distribution of sizes, shapes, and/or surface chemistries, Eqs. (4) must be averaged over a distribution, usually assumed to be Gaussian, of the frequency shift parameter δ. Eqs. (4) must also be averaged

over a Boltzmann distribution of initial phonon states $|I\rangle$ if the ground-state phonon frequency is not large compared with k_BT, and over contributions from different phonon transitions that are nearly degenerate and therefore cannot be distinguished experimentally. For example, the main Raman transition in CdSe is referred to as the longitudinal optical (LO) phonon, but in fact many different LO phonons with different wavevectors and nearly identical frequencies may contribute to the spectrum. Considering both of these ensemble averaging effects, the expressions that correspond to what is actually measured in the laboratory are

$$\left[\frac{d\sigma(\omega_L,\omega_S)}{d\Omega}\right]_{||} = \sum_I P_I \int d\delta\, F(\delta) \left[\frac{d\sigma_{IF}(\omega_L,\delta)}{d\Omega}\right]_{||} \quad (6a)$$

$$\left[\frac{d\sigma(\omega_L,\omega_S)}{d\Omega}\right]_{\perp} = \sum_I P_I \int d\delta\, F(\delta) \left[\frac{d\sigma_{IF}(\omega_L,\delta)}{d\Omega}\right]_{\perp} \quad (6b)$$

where P_I is the initial thermal equilibrium population of phonon mode I and $F(\delta)$ is the Gaussian distribution of frequency shifts δ. If there is no polarization selection in the detection step, as we assume here, the sum of (6a) and (6b) is measured.

Finally, the corresponding electronic absorption spectrum is given in SI units by[36,39]

$$\sigma_A(\omega) = \frac{\omega}{3n\varepsilon_0\hbar c} \sum_I P_I \sum_e M_e^2 \int d\delta\, F(\delta)\, Re \int_0^\infty dt\, \langle I|I(t)\rangle_e exp\left[i\left(\omega - \omega_{eg} - \delta + \omega_I\right)t - g_e(t)\right] \quad (7)$$

where n is the solvent refractive index and *Re* designates the real part of the complex quantity. Note that the absorption spectrum and the resonance Raman profiles depend on all of the same material parameters, so any reasonable model for the spectroscopy must fit both experimental observables with the same set of parameters.

3. RESULTS

The overtone to fundamental Raman intensity ratio was calculated as a function of excitation frequency (ω_L) for five different electron-phonon coupling strengths and for three different ratios between the homogeneous (Brownian oscillator) and inhomogeneous linewidths, holding the total width constant. The Huang-Rhys factors varied from 0.02 to 0.72, roughly the range that has been reported for the LO phonon of CdSe nanocrystals through different experimental techniques.[5,17,20,41-46] The Brownian oscillator parameter κ, which has the effect of varying the homogeneous lineshape from Lorentzian to Gaussian (exponential to Gaussian decay in the time domain), was set to 0.01, producing a nearly Gaussian lineshape. Calculations were performed for a single resonant electronic state as well as for two states separated by 807 cm^{-1} (0.1 eV) with either parallel or perpendicular transition dipole directions. In each case, the total (homogeneous plus inhomogeneous) width was fixed at 960 cm^{-1} (FWHM), roughly the experimental absorption width of the lowest excitonic transition of good quality CdSe quantum dot preparations. The vibrational frequency was set to 208 cm^{-1}, appropriate for the LO phonon of CdSe, the temperature was fixed at 298 K, and the electronic transition frequency (for the lower of the two transitions in two-state calculations) was fixed at 18000 cm^{-1}. In each case the overtone to fundamental ratios are presented only for excitation frequencies at which there is significant absorbance, corresponding to a true resonance Raman process.

Figures 1-4 present the calculated absorption spectra and overtone to fundamental intensity ratio profiles. The absorption spectrum broadens slightly as the Huang-Rhys factor is increased, but this is a fairly small effect because vibronic structure is not the dominant source of breadth in these spectra. Several generalizations can be drawn from the calculated I_{2LO}/I_{LO}

ratios. In general the overtone to fundamental ratio does increase with increasing S, but there is not a direct proportionality and the increase tends to "saturate" for large S. The overtone to fundamental ratio also decreases as the contribution of homogeneous broadening to the absorption bandwidth increases. This is because more rapid homogeneous dephasing gives the initial ground-state phonon wavepacket less time to propagate on the excited-state potential energy surface [refer to eq. (5)], and the overlap $\langle F|I(t)\rangle$ takes longer to develop when I and F differ by two quanta than when they differ by only one. The overtone to fundamental ratio also varies considerably with excitation wavelength and, at least for fairly small S, is larger when excited on the higher-energy side of the absorption band. This can be understood most easily by reference to the sum-over-states formulation of the Raman amplitude [eqs. (2) and (3)]. For $0 \rightarrow 1$ fundamental scattering, $V = 0$ and $V = 1$ make almost all of the contribution to the total amplitude for small S, while for $0 \rightarrow 2$ scattering there is also a significant contribution from $V = 2$. This will tend to shift the overtone's excitation profile to higher energies relative to the fundamental profile.

Comparison of Figs. 1 and 2 shows that overlapping electronic transitions affect the overtone intensities even if both transitions have identical broadening parameters and Huang-Rhys factors. The differences are most pronounced when the homogeneous broadening is largest. This occurs because the contributions from the two transitions can interfere either constructively or destructively at the level of the Raman amplitude [eq. (5)], and the interference patterns for the overtone and the fundamental are somewhat different. Figs. 3 and 4 show the effect of overlap between the transition of interest and a transition with lower oscillator strength

but a relatively large Huang-Rhys factor when the two transitions are either polarized in the same direction (Fig. 3) or in perpendicular directions (Fig. 4).

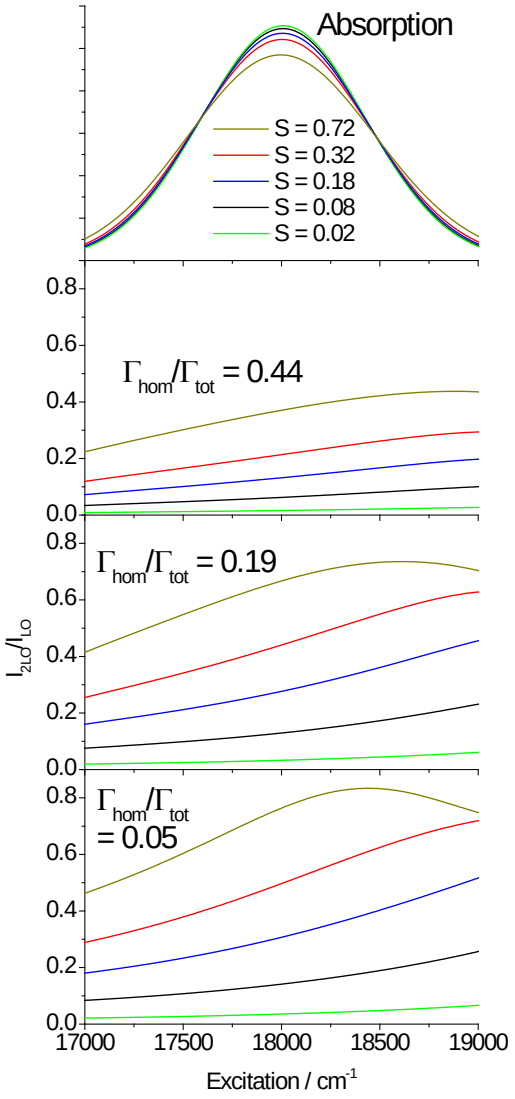

Figure 1. Absorption spectrum and overtone to fundamental intensity ratios as a function of the Huang-Rhys factor S for a single resonant electronic state. Three different ratios of homogeneous to total electronic spectral width are shown.

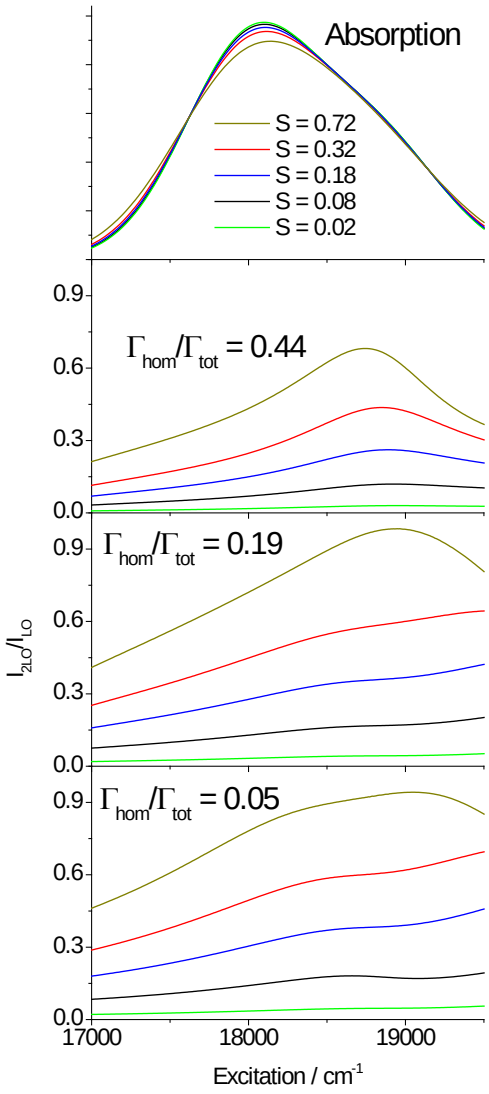

Figure 2: Same as Fig. 1 but for two resonant electronic states having the same polarization and Huang-Rhys factor. The two states are separated by 807 cm^{-1} and the lower-energy state has twice the oscillator strength of the higher-energy state.

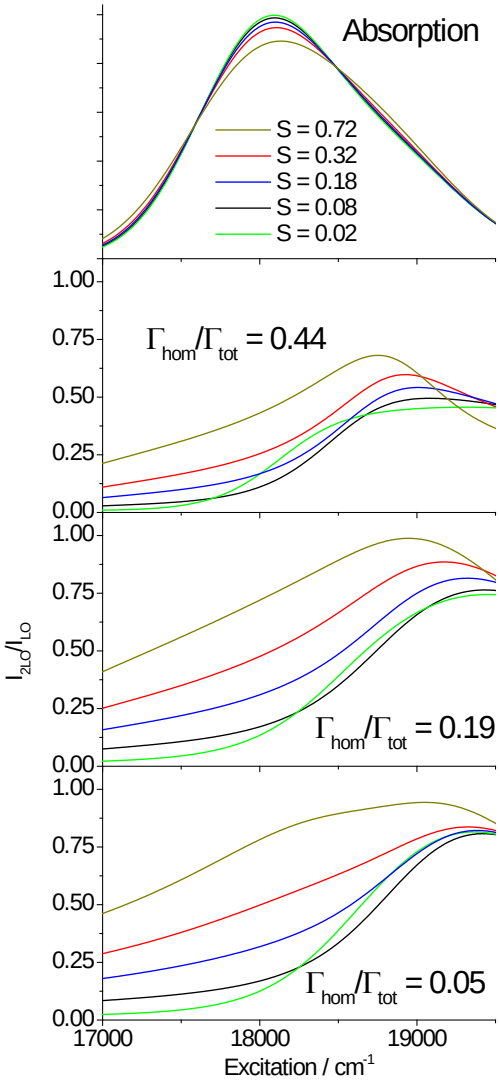

Figure 3: Absorption spectrum and overtone to fundamental intensity ratios for two resonant electronic states with the same polarization and separated by 807 cm^{-1}, with the higher-energy state having half the oscillator strength of the lower-energy state. The higher-energy state has a fixed Huang-Rhys factor of 0.72 while S for the lower state is varied as shown.

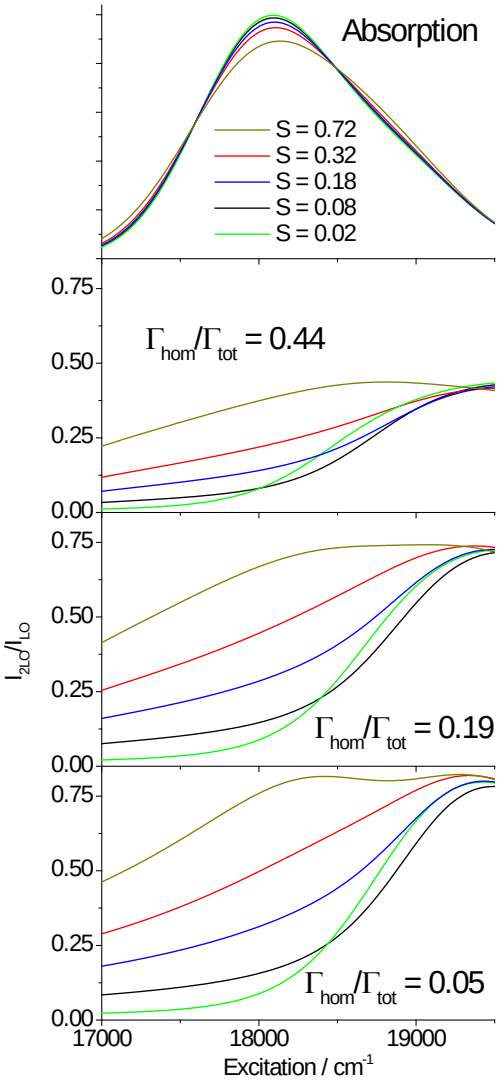

Figure 4: Same as Fig. 3 except that the lower-energy state is z-polarized while the higher-energy state is xy-polarized.

Figure 5 plots the intensity ratios obtained with excitation at the absorption maximum for the largest and smallest homogeneous to inhomogeneous broadening ratios considered. This figure shows the sub-linear scaling of overtone to fundamental ratio with S for fixed linewidth, as well as the reduction in overtone intensity as the homogeneous contribution to the linewidth is increased at fixed S. In addition, this plot shows that when the electronic transition of interest is partially overlapped by a weaker transition having large EPC, increasing S can actually decrease the overtone to fundamental ratio even if the dephasing rate is fixed and excitation is at the peak of the absorption band. This is also directly apparent in Figs. 3 and 4, where the green curve (S = 0.02) is above the blue and black ones (S = 0.18 and 0.08) in certain excitation ranges. This occurs because the contributions to the fundamental intensity interfere destructively in this region, while the overtone intensity arises almost entirely from the higher energy, larger S state.

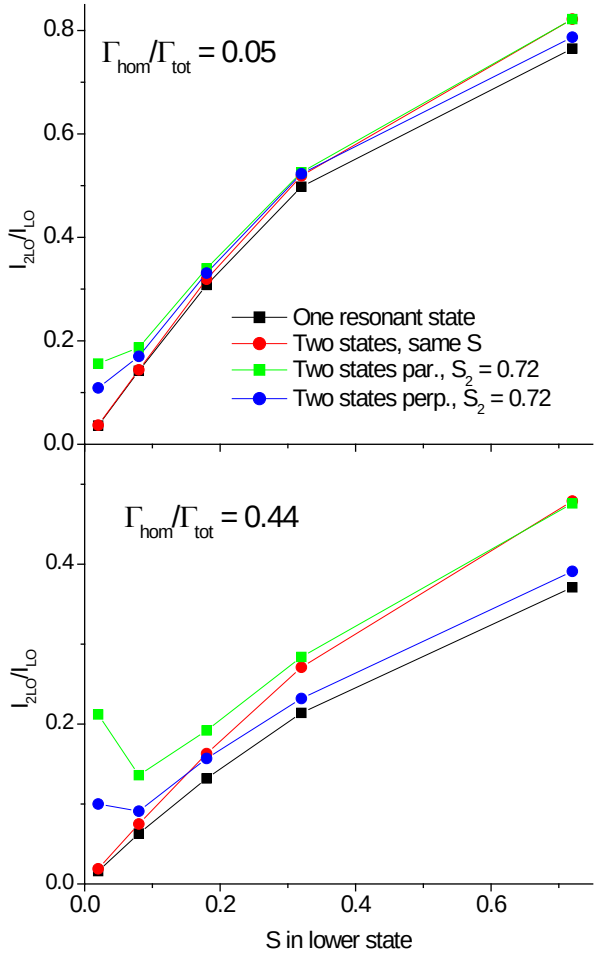

Figure 5. LO overtone to fundamental intensity ratio obtained with excitation at the maximum of the absorption spectrum as a function of the Huang-Rhys factor in the lower-energy state (the one that makes the dominant contribution to the absorbance at the maximum) for two different values of the homogeneous to total linewidth ratio (total width 960 cm^{-1}). The four colors represent the four choices of polarization and Huang-Rhys factor for the higher-energy transition considered in Figures 1-4.

4. DISCUSSION

Table I summarizes some reported experimental values of the overtone to fundamental intensity ratio in CdSe nanocrystals, the conditions under which the measurements were made, and the conclusions reached about electron-phonon coupling strengths. In view of the different sizes and surface treatments of the nanocrystals and the highly variable experimental

conditions, the overtone to fundamental ratio is quite consistent from one experiment to another; however, in those cases where a Huang-Rhys factor was reported, these span a considerably larger range. The results of the simulations presented here suggest that, with the exception of the very small values obtained by Lange,[8] any of the S values in Table 1 could be consistent with the reported overtone intensities depending on the actual value of the homogeneous linewidth and the extent of overlap among resonant states.

Table 1. Literature values of Raman overtone to fundamental intensity ratio and its interpretation for CdSe nanocrystals.

material	$\frac{I_2}{I_1}$	conditions	reported conclusions	ref.
CdSe and CdSe/ZnS core-shell rods, varying diameter	0.45-0.38 (core) 0.25-0.33 (core-shell)	514 nm exc, liq He temp	S = 0.053-0.044 (core), 0.030-0.036 (core-shell)	8
CdSe/ZnS core-shell dots, 4 nm diam core	0.2	476.5 nm exc, room temp, on Si wafer	S ≈ 0.2	20
CdSe dots, 4.5 nm diam	0.33	514.5 nm exc, polymer film, 1.6 K	S = 0.5	5
CdSe nanoparticles, 2-5 nm diam (polydisperse sample)	0.3-0.4	442-529 nm exc, gelatin or polymer film, room temp	S varies negligibly with diameter	47
CdSe dots, 5.4 nm diam	0.3-0.4	514.5 nm exc	S >> 0.025	44
CdSe-doped glasses, 4-8 nm diam (polydisperse)	~0.37	476-568 nm exc, 77 K	S = 0.5-0.9	6

The homogeneous linewidths used in these calculations have been chosen to span the range likely to be appropriate for CdSe nanocrystals near room temperature. At low excitation intensities, observed linewidths for the lowest excitonic transition of single nanocrystals are on

the order of 1-2 cm^{-1} at 3-10 K[15,48,49] and less than 0.1 cm^{-1} at a lower temperature,[50] but it is not clear how to extrapolate these results to higher temperatures. Older photon echo measurements yielded a homogeneous linewidth of ~50 cm^{-1} at 15 K with only a modest temperature dependence up to 160 K.[41] The smallest homogeneous width used in the calculations shown here is 48 cm^{-1} full width at half maximum, and further reducing it has almost no effect on the overtone to fundamental intensity ratio; the dephasing is slow compared with the phonon frequency, and $\langle 2|0(t)\rangle$ does not experience significantly more damping than $\langle 1|0(t)\rangle$. Increasing the homogeneous width above the largest value used here does further reduce the overtone to fundamental ratio for any given value of S, and at least one three-pulse photon echo study suggests that the homogeneous broadening may account for more than half the width of the lowest excitonic transition at room temperature.[51] Larger homogeneous widths may also be appropriate for the higher-energy transitions.

The results of these resonance Raman intensity simulations clearly demonstrate that Huang-Rhys factors may be obtained from Raman overtone intensities only under some very limiting conditions: a single electronic transition contributes to the resonance Raman intensity, the excitation wavelength is at or near the maximum of the inhomogeneously broadened absorption band, and the homogeneous linewidth is small compared with the phonon frequency of interest. When those conditions are met, as in the black curve of Fig. 5 (top), the Raman overtone to fundamental ratio is given quite accurately as a quadratic function of the Huang-Rhys parameter,

$$\frac{I_2}{I_1} = 1.95S - 1.15S^2 \qquad (8)$$

This equation reproduces the data to within better than 5% under the stated conditions. While this simple relationship is easy to apply, it may be far from correct if any of the conditions for its validity are not met.

Often one is interested less in the absolute magnitude of the electron-phonon coupling than in how it changes as some parameter of the material (size, shape, surface chemistry) is varied. If the resonance condition and homogeneous width are constant and a single electronic state dominates the resonance enhancement, the overtone to fundamental ratio does increase monotonically with *S*. Maintaining a constant resonance condition is straightforward in principle, although a continuously tunable excitation source is not always available. However, changing the size, shape, or surface chemistry of a nanocrystal may also affect the linewidths as well as the relative positions and/or intensities of other electronic transitions that partially overlap the one of interest and influence the Raman intensities. Thus, one cannot necessarily conclude that an increased relative overtone intensity signifies stronger EPC.

ACKNOWLEDGEMENTS

This work was supported by NSF grant #CHE-1112192.

REFERENCES

1. Shiang, J. J.; Risbud, S. H.; Alivisatos, A. P. Resonance Raman Studies of the Ground and Lowest Electronic Excited State in CdS Nanocrystals *J. Chem. Phys.* **1993**, *98*, 8432-8442.

2. Zhang, Q.; Zhang, J.; Utama, M. I. B.; Peng, B.; de la Mata, M.; Arbiol, J.; Xiong, Q. Exciton-Phonon Coupling in Individual ZnTe Nanorods Studied by Resonant Raman Spectroscopy *Phys. Rev. B* **2012**, *85*, 085418.

3. Myers, A. B.; Mathies, R. A. Resonance Raman Intensities: A Probe of Excited-State Structure and Dynamics. In *Biological Applications of Raman Spectroscopy*; Spiro, T. G., Ed.; Wiley: New York, 1987; Vol. 2; pp 1-58.

4. Myers, A. B. Excited Electronic State Properties from Ground-State Resonance Raman Intensities. In *Laser Techniques in Chemistry*; Myers, A. B., Rizzo, T. R., Eds.; Wiley: New York, 1995; pp 325-384.

5. Alivisatos, A. P.; Harris, T. D.; Carroll, P. J.; Steigerwald, M. L.; Brus, L. E. Electron-Vibration Coupling in Semiconductor Clusters Studied by Resonance Raman Spectroscopy *J. Chem. Phys.* **1989**, *90*, 3463-3468.

6. Klein, M. C.; Hache, F.; Ricard, D.; Flytzanis, C. Size Dependence of Electron-Phonon Coupling in Semiconductor Nanospheres: The Case of CdSe *Phys. Rev. B* **1990**, *42*, 11123-11132.

7. Krauss, T. D.; Wise, F. W. Raman-Scattering Study of Exciton-Phonon Coupling in PbS Nanocrystals *Phys. Rev. B* **1997**, *55*, 9860-9865.

8. Lange, H.; Artemyev, M.; Woggon, U.; Niermann, T.; Thomsen, C. Experimental Investigation of Exciton-LO-Phonon Couplings in CdSe/ZnS Core/Shell Nanorods *Phys. Rev. B* **2008**, *77*, 193303.

9. Pandey, A.; Guyot-Sionnest, P. Slow Electron Cooling in Colloidal Quantum Dots *Science* **2008**, *322*, 929-932.

10. Klimov, V. I. Spectral and Dynamical Properties of Multiexcitons in Semiconductor Nanocrystals *Ann. Rev. Phys. Chem.* **2007**, *58*, 635-673.

11. Kambhampati, P. Hot Exciton Relaxation Dynamics in Semiconductor Quantum Dots: Radiationless Transitions on the Nanoscale *J. Phys. Chem. C* **2011**, *115*, 22089–22109.

12. Kambhampati, P. Unraveling the Structure and Dynamics of Excitons in Semiconductor Quantum Dots *Acc. Chem. Res.* **2012**, *44*, 1-13.

13. Beard, M. C.; Midgett, A. G.; Hanna, M. C.; Luther, J. M.; Hughes, B. K.; Nozik, A. J. Comparing Multiple Exciton Generation in Quantum Dots to Impact Ionization in Bulk Semiconductors: Implications for Enhancement of Solar Energy Conversion *Nano Lett.* **2010**, *10*, 3019-3027.

14. Boulesbaa, A.; Issac, A.; Stockwell, D.; Huang, Z.; Huang, J.; Guo, J.; Lian, T. Ultrafast Charge Separation at CdS Quantum Dot/Rhodamine B Molecule Interface *J. Am. Chem. Soc.* **2007**, *129*, 15132-15133.

15. Fernée, M. J.; Littleton, B. N.; Cooper, S.; Rubinsztein-Dunlop, H.; Gomez, D. E.; Mulvaney, P. Acoustic Phonon Contributions to the Emission Spectrum of Single CdSe Nanocrystals *J. Phys. Chem. C* **2008**, *112*, 1878-1884.

16. Martin, J.; Cichos, F.; Huisken, F.; von Borczyskowski, C. Electron-Phonon Coupling and Localization of Excitons in Single Silicon Nanocrystals *Nano Lett.* **2008**, *8*, 656-660.

17. Groeneveld, E.; de Mello Donegá, C. Enhanced Exciton–Phonon Coupling in Colloidal Type-II CdTe-CdSe Heteronanocrystals *J. Phys. Chem. C* **2012**, *116*, 16240–16250.

18. Norris, D. J.; Efros, A. L.; Rosen, M.; Bawendi, M. G. Size Dependence of Exciton Fine Structure in CdSe Quantum Dots *Phys. Rev. B* **1996**, *53*, 16347-16354.

19. Heitz, R.; Mukhametzhanov, I.; Stier, O.; Madhukar, A.; Bimberg, D. Enhanced Polar Exciton-LO-Phonon Interaction in Quantum Dots *Phys. Rev. Lett.* **1999**, *83*, 4654-4657.

20. Baranov, A. V.; Rakovich, Y. P.; Donegan, J. F.; Perova, T. S.; Moore, R. A.; Talapin, D. V.; Rogach, A. L.; Masumoto, Y.; Nabiev, I. Effect of ZnS Shell Thickness on the Phonon Spectra in CdSe Quantum Dots *Phys. Rev. B* **2003**, *68*, 165306.

21. Seong, M. J.; Micic, O. I.; Nozik, A. J.; Mascarenhas, A.; Cheong, H. M. Size-Dependent Raman Study of InP Quantum Dots *Appl. Phys. Lett.* **2003**, *82*, 185-187.

22. Wang, R. P.; Xu, G.; Jin, P. Size Dependence of Electron-Phonon Coupling in ZnO Nanowires *Phys. Rev. B* **2004**, *69*, 113303.

23. Hsu, W.-T.; Lin, K.-F.; Hsieh, W.-F. Reducing Exciton-Longitudinal-Optical-Phonon Interaction with Shrinking ZnO Quantum Dots *Appl. Phys Lett.* **2007**, *91*, 181913.

24. Zeiri, L.; Patla, I.; Acharya, S.; Golan, Y.; Efrima, S. Raman Spectroscopy of Ultranarrow CdS Nanostructures *J. Phys. Chem. C* **2007**, *111*, 11843-11848.

25. Dzhagan, V. M.; Valakh, M. Y.; Raevska, O. E.; Stroyuk, O. L.; Kuchmiy, S. Y.; Zahn, D. R. T. The Influence of Shell Parameters on Phonons in Core-Shell Nanoparticles: A Resonant Raman Study *Nanotechnology* **2009**, *20*, 365704.

26. Fan, D.; Zhang, R.; Zhu, Y.; Peng, H. Size Dependence of Surface Optical Mode and Electron-Phonon Coupling in ZnO Nanocombs *Physica B* **2012**, *407*, 3510-3514.

27. Chinsky, L.; Laigle, A.; Peticolas, W. L.; Turpin, P.-Y. Excited State Geometry of Uracil from the Resonant Raman Overtone Spectrum Using a Kramers-Kronig Technique *J. Chem. Phys.* **1982**, *76*, 1-5.

28. Merlin, R.; Guntherodt, G.; Humphreys, R.; Cardona, M.; Suryanarayanan, R.; Holtzberg, F. Multiphonon Processes in YbS *Phys. Rev. B* **1978**, *17*, 4951-4958.

29. Myers, A. B. Molecular Electronic Spectral Broadening in Liquids and Glasses *Ann. Rev. Phys. Chem.* **1998**, *49*, 267-295.

30. Li, B.; Johnson, A. E.; Mukamel, S.; Myers, A. B. The Brownian Oscillator Model for Solvation Effects in Resonance Raman and Emission Spectroscopies and Their Relationship to Electron Transfer *J. Am. Chem. Soc* **1994**, *116*, 11039-11047.

31. Sue, J.; Yan, Y. J.; Mukamel, S. Raman Excitation Profiles of Polyatomic Molecules in Condensed Phases. A Stochastic Theory *J. Chem. Phys.* **1986**, *85*, 462-474.

32. Yan, Y. J.; Mukamel, S. Molecular Fluorescence and near Resonance Raman Yield as a Probe for Solvation Dynamics *J. Chem. Phys.* **1987**, *86*, 6085-6107.

33. Myers, A. B. "Time-Dependent" Resonance Raman Theory *J. Raman Spectrosc.* **1997**, *28*, 389-401.

34. Myers, A. B.; Mathies, R. A.; Tannor, D. J.; Heller, E. J. Excited State Geometry Changes from Preresonance Raman Intensities: Isoprene and Hexatriene *J. Chem. Phys.* **1982**, *77*, 3857-3866.

35. Kelley, A. M. Resonance Raman and Resonance Hyper-Raman Intensities: Structure and Dynamics of Molecular Excited States in Solution *J. Phys. Chem. A* **2008**, *112*, 11975-11991.

36. Phillips, D. L.; Myers, A. B. Photodissociation of Alkyl Iodides in Solution: Substituent Effects on the Early Time Dynamics *J. Chem. Phys.* **1991**, *95*, 226-243.

37. Shiang, J. J.; Kadavanich, A. V.; Grubbs, R. K.; Alivisatos, A. P. Symmetry of Annealed Wurtzite CdSe Nanocrystals: Assignment to the C_{3v} Point Group *J. Phys. Chem.* **1995**, *99*, 17417-17422.

38. Sension, R. J.; Strauss, H. L. Comparison of Experiment and Theory for the Resonance Raman Spectrum of I_2 in Solution. I. The Raman Excitation Profile of I_2 in n-Hexane *J. Chem. Phys.* **1986**, *85*, 3791-3806.

39. Kelley, A. M. *Condensed Phase Molecular Spectroscopy and Photophysics*; John Wiley & Sons: Hoboken, NJ, 2013.

40. Mukamel, S. *Principles of Nonlinear Optical Spectroscopy*; Oxford University Press: New York, 1995.

41. Mittleman, D. M.; Schoenlein, R. W.; Shiang, J. J.; Colvin, V. L.; Alivisatos, A. P.; Shank, C. V. Quantum Size Dependence of Femtosecond Electronic Dephasing and Vibrational Dynamics in CdSe Nanocrystals *Phys. Rev. B* **1994**, *49*, 14435-14447.

42. Norris, D. J.; Bawendi, M. G. Measurement and Assignment of the Size-Dependent Optical Spectrum in CdSe Quantum Dots *Phys. Rev. B* **1996**, *53*, 16338-16346.

43. Salvador, M. R.; Graham, M. W.; Scholes, G. D. Exciton-Phonon Coupling and Disorder in the Excited States of CdSe Colloidal Quantum Dots *J. Chem. Phys.* **2006**, *125*, 184709.

44. Sagar, D. M.; Cooney, R. R.; Sewall, S. L.; Dias, E. A.; Barsan, M. M.; Butler, I. S.; Kambhampati, P. Size Dependent, State-Resolved Studies of Exciton-Phonon Couplings in Strongly Confined Semiconductor Quantum Dots *Phys. Rev. B* **2008**, *77*, 235321.

45. Sagar, D. M.; Cooney, R. R.; Sewall, S. L.; Kambhampati, P. State-Resolved Exciton-Phonon Couplings in CdSe Semiconductor Quantum Dots *J. Phys. Chem. C* **2008**, *112*, 9124-9127.

46. McKimmie, L. J.; Lincoln, C. N.; Jasieniak, J.; Smith, T. A. Three-Pulse Photon Echo Peak Shift Measurements of Capped CdSe Quantum Dots *J. Phys. Chem. C* **2010**, *114*, 82–88.

47. Dzhagan, V. M.; Valakh, M. Y.; Raevskaya, A. E.; Stroyuk, A. L.; Kuchmiy, S. Y.; Zahn, D. R. T. Size Effects on Raman Spectra of Small CdSe Nanoparticles in Polymer Films *Nanotechnology* **2008**, *19*, 305707.

48. Empedocles, S. A.; Norris, D. J.; Bawendi, M. G. Photoluminescence Spectroscopy of Single CdSe Nanocrystallite Quantum Dots *Phys. Rev. Lett.* **1996**, *77*, 3873-3876.

49. Chilla, G.; Kipp, T.; Menke, T.; Heitmann, D.; Nikolic, M.; Fromsdorf, A.; Kornowski, A.; Forster, S.; Weller, H. Direct Observation of Confined Acoustic Phonons in the Photoluminescence Spectra of a Single CdSe-CdS-ZnS Core-Shell-Shell Nanocrystal *Phys. Rev. Lett.* **2008**, *100*, 057403.

50. Biadala, L.; Louyer, Y.; Tamarat, P.; Lounis, B. Direct Observation of the Two Lowest Exciton Zero-Phonon Lines in Single CdSe/ZnS Nanocrystals *Phys. Rev. Lett.* **2009**, *103*, 037404.

51. Salvador, M. R.; Hines, M. A.; Scholes, G. D. Exciton-Bath Coupling and Inhomogeneous Broadening in the Optical Spectroscopy of Semiconductor Quantum Dots *J. Chem. Phys.* **2003**, *118*, 9380-9387.

Table of Contents graphic